Kato S, Akimoto K, Nagashima Y, Ishiguro H, Kubota K, Kobayashi N, Hosono K, Watanabe S, Sekino Y, Sato T, Sasaki K, Nakaigawa N, Kubota Y, Inayama Y, Endo I, Ohno S, Maeda S, Nakajima A.	aPKCλ/ι is a beneficial prognostic marker for pancreatic neoplasms.	Pancreatology	13(4)	360-8	2013
Watanabe S, Sato T, Kato S, Hosono K, Kobayashi N, Nakajima A, Kubota K.	Positioning of nasobiliary tube using magnet-loaded catheters	Endoscopy	45(10)	835-7	2013
Tomeno W, Yoneda M, Imajo K, Ogawa Y, Kessoku T, Saito S, Eguchi Y, Nakajima A.	Emerging drugs for non-alcoholic steatohepatitis	Expert Opin Emerg Drugs	18(3)	279-90	2013
Kato S, Akimoto K, Nagashima Y, Ishiguro H, Kubota K, Kobayashi N, Hosono K, Watanabe S, Sekino Y, Sato T, Sasaki K, Nakaigawa N, Kubota Y, Inayama Y, Endo I, Ohno S, Maeda S, Nakajima A.	aPKCλ/ι is a beneficial prognostic marker for pancreatic neoplasms.	Pancreatology	13(4)	360-8	2013

Genetic reconstitution of tumorigenesis in primary intestinal cells

Kunishige Onuma[a], Masako Ochiai[a], Kaoru Orihashi[a], Mami Takahashi[b], Toshio Imai[b], Hitoshi Nakagama[a], and Yoshitaka Hippo[a,1]

[a]Division of Cancer Development System and [b]Central Animal Division, National Cancer Center Research Institute, Tokyo 104-0045, Japan

Edited by Bert Vogelstein, Johns Hopkins University, Baltimore, MD, and approved May 28, 2013 (received for review December 17, 2012)

Animal models for human colorectal cancer recapitulate multistep carcinogenesis that is typically initiated by activation of the Wnt pathway. Although potential roles of both genetic and environmental modifiers have been extensively investigated in vivo, it remains elusive whether epithelial cells definitely require interaction with stromal cells or microflora for tumor development. Here we show that tumor development could be simply induced independently of intestinal microenvironment, even with WT murine primary intestinal cells alone. We developed an efficient method for lentiviral transduction of intestinal organoids in 3D culture. Despite seemingly antiproliferative effects by knockdown of adenomatous polyposis coli (*APC*), we managed to reproducibly induce *APC*-inactivated intestinal organoids. As predicted, these organoids were constitutively active in the Wnt signaling pathway and proved tumorigenic when injected into nude mice, yielding highly proliferative tubular epithelial glands accompanied by prominent stromal tissue. Consistent with cellular transformation, tumor-derived epithelial cells acquired sphere formation potential, gave rise to secondary tumors on retransplantation, and highly expressed cancer stem cell markers. Inactivation of *p53* or phosphatase and tensin homolog deleted from chromosome 10, or activation of *Kras*, promoted tumor development only in the context of *APC* suppression, consistent with earlier genetic studies. These findings clearly indicated that genetic cooperation for intestinal tumorigenesis could be essentially recapitulated in intestinal organoids without generating gene-modified mice. Taken together, this in vitro model for colon cancer described herein could potentially provide unique opportunities for carcinogenesis studies by serving as a substitute or complement to the currently standard approaches.

colon carcinogenesis | shRNA | primary culture | Matrigel | validation

Accumulation of multiple genetic alterations underlies colon carcinogenesis, in which inactivation of adenomatous polyposis coli (*APC*) is an initiating event leading to the development of adenoma in most sporadic cases (1). Both *APC* inactivation and an activating mutation in the *CTNNB1* gene encoding β-catenin result in β-catenin accumulation through inhibition of its degradation, leading to constitutive activation of the Wnt pathway that is transcriptionally regulated by the β-catenin/transcription factor 4 (TCF) complex (2).

Widely used animal models for colorectal cancer (CRC) recapitulate tumor development in a similar manner. One is a mouse genetic model with a mutant allele of *APC*. Typically, multiple adenomas spontaneously develop predominantly in the small intestine through inactivation of the remaining allele (3, 4). The other is a chemically induced carcinogenesis model. Administration of azoxymethane (AOM) or a dietary carcinogen, 2-amino-1-methyl-6-phenylimidazo [4,5-*b*] pyridine (PhIP), recapitulates colon carcinogenesis in rodents by introducing an activating mutation in *CTNNB1* (5, 6) or inactivating *APC*, by mutation (7) or post-transcriptional down-regulation by overexpressed staphylococcal nuclease and tudor domain containing 1 (*SND1*) (8). Potential roles of genetic or environmental factors have been extensively investigated with these models. For instance, disruption of *p53* (9, 10) or phosphatase and tensin homolog deleted from chromosome 10 (*PTEN*) (11, 12) or induction of oncogenic *Kras* (13–15) significantly promoted intestinal tumorigenesis only in the context of *APC* loss. Protumorigenic effects by active inflammation have been demonstrated by inducing colitis with dextran sodium sulfate (DSS) (16). Conversely, critical roles of microflora and basal inflammation underlying tumorigenesis were also demonstrated by genetic ablation of *Myd88* (17) and *STAT3* (18), key genes in the innate immunity and inflammation, respectively.

Recent genomic and expression profile analyses have revealed a huge number of genes with mutation, deletion, or aberrant expression in human CRC (19, 20). Forward genetic screens in mice have also identified a number of genes potentially involved in intestinal tumorigenesis (21). Candidate genes for CRC have been usually validated through generation of gene-modified mice. However, it might be unrealistic to take this approach for very many genes, given the amount of time and work required for the analysis of each gene. This situation is especially true if generation of conditional KO mice and intercrossing between multiple strains becomes necessary. Alternatively, functional analyses of the genes have been widely conducted in colon cancer cell lines and fibroblasts to investigate the relevance in tumor progression and to determine oncogenic potential, respectively. However, the results might not be directly extrapolated to early stages of intestinal tumorigenesis, underscoring the definite requirement for simple validation methods in normal intestinal cells.

Given that intestinal stem cells efficiently give rise to adenoma on activation of the Wnt pathway in vivo (22, 23), we postulated that a similar approach might induce tumor development in vitro, although the requirements of intestinal microenvironment remained elusive. With recent advances in long-term culture of intestinal stem cells (24), we set out to suppress *APC* in intestinal organoids with a lentivirus. We generated tumors from intestinal organoids, independently of the in vivo setting and without using gene-modified mice. Representative genetic cooperation for tumorigenesis could be recapitulated by taking this approach, likely establishing an in vitro model for CRC.

Results

Lentivirus-Based Efficient and Stable Gene Delivery to Intestinal Organoids. To reconstitute tumorigenesis in vitro, stem cells need to be stably transduced. We adopted lentiviral gene delivery for its high infection efficiency to primary cells, including quiescent stem cells (25). However, it was revealed that Matrigel inhibited viral transduction of intestinal epithelial cells (IECs) in 3D culture, despite its definite requirement for survival. To satisfy both the presence of Matrigel and accessibility to lentiviral

Author contributions: H.N. and Y.H. designed research; K. Onuma, M.O., K. Orihashi, and Y.H. performed research; M.T. contributed new reagents/analytic tools; T.I. analyzed data; and Y.H. wrote the paper.

The authors declare no conflict of interest.

This article is a PNAS Direct Submission.

[1]To whom correspondence should be addressed. E-mail: yhippo@ncc.go.jp.

This article contains supporting information online at www.pnas.org/lookup/suppl/doi:10.1073/pnas.1221926110/-/DCSupplemental.

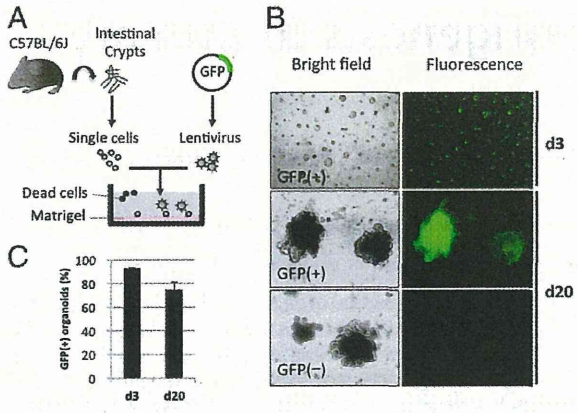

Fig. 1. Stable gene transduction of IECs in 3D culture. (*A*) Schematic diagram for lentiviral infection. Intestinal crypts isolated from C57BL/6J mice were dissociated into single cells and incubated with lentiviral particles encoding GFP for 16 h on Matrigel. (*B*) Stable and efficient transduction of organoids. Transduced organoids at day 3, at 40× magnification (*Top*). At day 20, transduced organoids consisting of GFP-positive cells (*Middle*). A non-GFP vector gave rise to only faint auto-fluorescence by dead cells at 100× magnification (*Bottom*). Representative images are shown. (*C*) Transduction efficiency to intestinal cells. Rate for GFP-positive organoids without drug selection is shown. GFP-positive and -negative organoids were counted under a microscope 48 h after the infection (day 3) or second subculture (day 20). Mean ± SD (n = 3) is shown.

particles, we coincubated dissociated single cells and viral particles on Matrigel (Fig. 1*A*), which achieved high transduction efficiency (Fig. 1*B*). About half of the cells composing organoids were viable, and ~20% of them attached to Matrigel with or without viral particles (Fig. S1), whereas no dead cells were observed on Matrigel. Attached cells readily developed into tiny circular organoids at day 3 (Fig. 1*B*), implying this procedure might enable preferentially capture intestinal cells of a highly proliferative nature. Even without drug selection, the GFP-positive rate was as high as 93% at day 3, which fell to 75% at day 20 (Fig. 1*C*), presumably due to slightly adverse effects by viral integration. Many organoids consisted of only GFP-positive cells at day 20, even after two rounds of subculture (Fig. 1*B*). Given the rapid turnover rate of IECs (24), we reasoned that organoids were likely reconstituted by stably transduced stem cells.

Wnt Pathway Activation in Organoids Transduced with Multiple Clones of shRNA Against *APC*. With this efficient technique, we introduced a total of five clones of potent shRNA against *APC* (shAPC) (Fig. S2*A*) individually into organoids. With a routine schedule for 3D culture (Fig. S2*B*), however, we frequently failed in propagation for any shAPC clone tested, even under drug selection (Fig. S2*C*), suggesting adverse effects by *APC* knockdown in vitro. In contrast, introduction of potent shp53 or shPTEN (Fig. S2*D*) resulted in steady propagation of organoids (Fig. 2*A*), which spontaneously became puro-resistant, suggesting a growth advantage of inactivating *p53* or *PTEN*. We later found that cointroducing all of the five shAPC clones together (hereafter referred to as shAPCs) reproducibly gave rise to rounded cystic organoids, which dominated the population over time (Fig. 2*A*; Fig. S2*C*). Similar structures have been previously documented for organoids from *APC*-deficient adenoma (26, 27), suggesting a link between the morphology and *APC* loss. However, we assumed that this might not be necessarily the case, because we knew that cystic shape could be induced independent of *APC* knockdown (e.g., under stressed culture conditions including freeze/thaw, drug selection, or too stringent dissociation), which prompted us to characterize the cystic organoids with shAPCs in more detail. We found that they were puro-resistant and indeed suppressed for expression of *APC* (Fig. S2*D*). In thin sections, they lost physiological properties such as polarity (Fig. 2*B*), differentiation (Fig. 2*C*), and cellular turnover (Fig. 2 *B* and *C*), consistent with perturbed differentiation and migration associated with *APC* inactivation (28). In addition, β-catenin accumulation indicative of Wnt pathway activation was evident (Fig. 2*D*), which was also confirmed by qPCR analysis demonstrating up-regulation of *Axin2* (Fig. 2*E*), a specific target of the β-catenin/TCF complex (29). These observations implied that the organoids with shAPCs might be essentially similar, if not identical, to those derived from *APC*-deficient adenoma.

Induction of Tumors from Organoids by RNAi-Mediated Suppression of *APC*. We next investigated whether suppression of *APC* in organoids could also lead to tumor development, as observed in adenoma in vivo. After 4 wk of culture, organoids with shAPCs corresponding to 5×10^5 cells were mixed with Matrigel and injected into nude mice. At 6 wk after injection, round and solid flesh-colored nodules frequently developed (Fig. 3*A*). They were characterized by epithelial glands and prominently infiltrated stromal cells (Fig. 3*B*). Active proliferation of epithelia was verified by high Ki-67 labeling index and inferred from β-catenin accumulation (Fig. 3*C*). Based on these features common to intestinal tumors, we classified them as "tumors." In contrast, organoids with the vector control gave rise to no nodules at all or small flat nodules with a gelatinous appearance, if any (Fig. 3*A*). As they histologically lacked epithelial glands (Fig. 3*B*), we classified them as "Matrigel plugs." In the absence of shAPCs, no tumor was induced by shp53 and/or shPTEN or from *p53*- and *PTEN*-deficient organoids (Fig. S3; Table 1), in line with earlier studies in vivo (11, 12, 30, 31). In some cases, organoids with

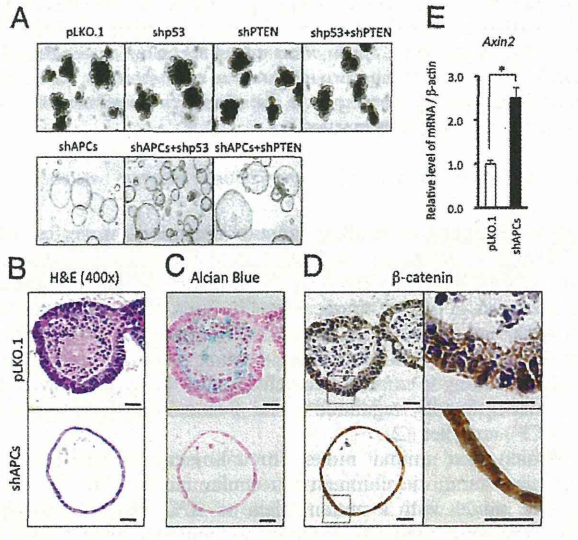

Fig. 2. RNAi-mediated suppression of *APC* in intestinal organoids. (*A*) Organoids transduced with various shRNA(s). Representative images at 4 wk after transduction are shown. Large rounded cysts were induced exclusively in the presence of shAPCs. pLKO.1 is an empty vector. (*B–D*) Transduced organoids in thin section. Serial sections were stained with H&E (*B*), Alcian blue (*C*), and β-catenin antibody (*D*). In organoids with shAPCs, intraluminal debris due to physiological turnover of intestinal cells is lost. Paneth cells stained red (*B*) and mucus stained blue (*C*) also became absent. Localization of β-catenin shifted from membrane to cytoplasm and nucleus (*D*). *Insets* in the left panel are enlarged in the right panel. (Scale bar, 20 μm.) (*E*) qPCR analysis of *Axin2* in transduced organoids. Relative expression level of mRNA to *β-actin* is shown. Mean ± SD (n = 3) is shown; $^*P < 0.01$.

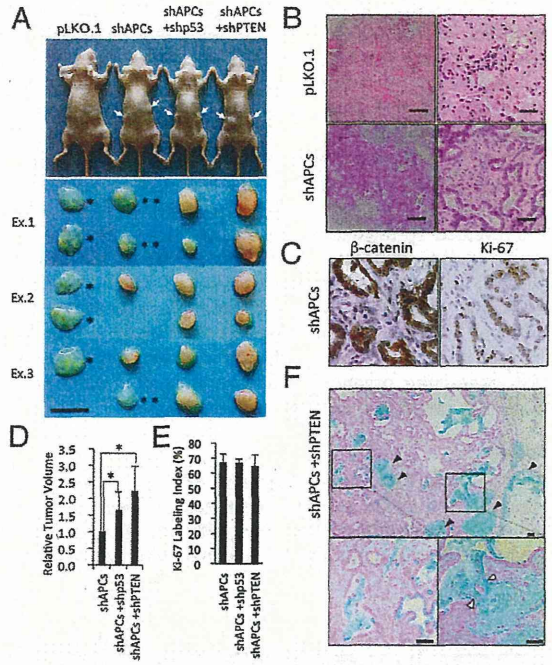

Fig. 3. RNAi-mediated induction of tumors from WT organoids. (*A*) s.c. tumors developed from injected organoids. Palpable nodules in nude mice (arrow) at 6 wk after injection (*Upper*). Excised nodules in three representative experiments (Ex.1–3). Matrigel plugs (asterisk), nontumor (double asterisks), or tumors (no asterisk) (*Lower*). (Scale bar, 10 mm.) (*B*) Histological features of the nodules. H&E staining of Matrigel plugs (*Upper*) and tumors with shAPCs alone (*Lower*) at 20× (*Left*) and 200× (*Right*) magnification. (Scale bar, 500 and 50 μm, respectively.) (*C*) Immunohistochemical analyses. Tumors with shAPCs alone stained for β-catenin (*Left*) and Ki-67 (*Right*). (Scale bar, 25 μm.) (*D*) Relative ratio of tumor volume. Mean ± SD ($n = 5$) is shown; $^*P < 0.05$. (*E*) Ki-67 labeling index for tumor epithelia. Mean ± SD ($n = 7$) is shown. (*F*) Alcian blue staining. Tumors with shAPCs+shPTEN were stained. Mucus pools stained in blue (closed arrowhead) in stroma (*Upper*). *Insets* are enlarged in lower panel. Mucus and cellular debris shed into the lumen (*Lower Left*) are leaking (open arrowhead) from the disrupted glands (*Lower Right*). (Scale bar, 50 μm.)

shAPCs alone comprised nodules resembling Matrigel plugs, but having focal white spots inside (Fig. 3*A*). We classified them as "nontumor," based on too low a proportion of epithelial cells. Thus, tumors were tentatively defined as nodules replacing coinjected Matrigel with proliferating epithelial glands at 6 wk after injection. By applying this criteria, the tumor development rate by shAPCs alone was 63% (=7/11), 5 cases for both sides and 2 cases for either side, among 11 cases (Table 1). These results suggested that *APC* suppression might be integral but not always sufficient for tumor development from organoids, consistent with earlier studies in vivo (17, 18, 32).

Suppression of *p53* or *PTEN* Promotes *APC*-Dependent Tumorigenesis from Organoids. Many gene-modified mice have been crossed with *APC* mutant mice to evaluate their impact on carcinogenesis, in which common readouts were multiplicity, size, and histology of the tumors. We wondered if similar analysis could be feasible at the cellular level. By cointroducing shp53 or shPTEN with shAPCs into organoids (Fig. 2*A*), tumor development was observed for both sides of nude mice in all of the cases tested (Fig. 3*A*; Table 1). Similar results were obtained by introduction of shAPCs into *p53*- (Fig. S3) and *PTEN*-deficient organoids (Table 1). A significant increase in tumor size was also observed (Fig. 3*D*), but an increase was not observed in proliferation index (Fig. 3*E*). No remarkable effects were detected in histological features, including mucus pool formation (Fig. 3*F*), tumor gland morphology (Fig. S4*A*), and β-catenin accumulation (Fig. S4*B*). Taken together, cooperation for tumorigenesis between *APC* loss and inactivation of either *p53* (9, 10) or *PTEN* (11, 12) could be recapitulated in tumors as an increase in size and development rate. We also verified that organoid culture was conducted in a stromal cell–free condition (Fig. S5), confirming tumorigenesis was indeed achieved with IECs alone.

Significant Acceleration of *APC*-Dependent Tumorigenesis from Organoids by *Kras* Activation. To reconstitute somatic mutation of *Kras*, which is frequent in human CRC (19), we deleted a stop codon flanked by two loxP elements [Lox-Stop-Lox (LSL)] blocking the expression of $Kras^{G12D}$ by lentiviral Cre-mediated recombination (33) in IECs from $Kras^{LSLG12D/+}$ mice (34, 35). Successful deletion was confirmed by detecting the "1-loxP" fragment (35) in genomic PCR (Fig. 4*A*). Amplification of the LSL cassette revealed its partial and complete deletion in organoids with Cre and shAPCs+Cre, respectively (Fig. 4*A*). On $Kras^{G12D}$ expression, active Ras enriched (Fig. 4*B*) without affecting the morphology of the organoids (Fig. 4*C*), verifying specific activation of Ras but not the Wnt pathway. We then asked whether a synergy between oncogenic *Kras* and *APC* loss in intestinal tumorigenesis (13–15) could be recapitulated in our model. Strikingly, organoids with shAPCs+Cre gave rise to tumors on both sides so rapidly that the nude mice became moribund at 2 wk after injection (Fig. 4*D*) in 11 of 11 cases (Fig. 4*E*). They typically appeared red, indicative of active angiogenesis and hemorrhage, and contained cystic dilatation due to retention of serous fluid (Fig. 4*D*). Compared with organoids with shAPCs alone, a significant increase in tumor size was observed (Fig. 4*F*). Cre did not synergize with shAPCs in $Kras^{+/+}$ organoids (Fig. S6), ruling out the possibility of direct synergy between Cre and shAPCs. Tumor glands became more densely packed with morphological alteration from an irregular cystic structure (Fig. 5 *B* and *E*) to a tubular or papillary structure (Fig. 5 *C* and *F*). Destruction of glands leading to mucus pool formation (Fig. 5*H*) disappeared, despite retained mucus production ability (Fig. 5*I*). Given no effects on both cell proliferation (Figs. 4*G* and 5 *K* and *L*) and the magnitude of β-catenin accumulation (Fig. 5 *N* and *O*), $Kras^{G12D}$ might have induced tumor growth through histological alterations. Thus, the synergy was successfully recapitulated in tumors as an increase in size and development rate and alteration in histology.

Marginal Effects by *Kras* Activation Alone on Tumorigenesis from Organoids. We also characterized nodules with either of shAPCs or $Kras^{G12D}$ at 2 wk postinjection for reference, although this was too early for the correct diagnosis. If the criteria for tumors were automatically applied, tumor-positive cases were seven of seven for shAPCs, three of seven for $Kras^{G12D}$, and zero of seven for pLKO.1 (Fig. 4*E*). Putative tumors induced by $Kras^{G12D}$ contained

Table 1. Summary of tumor development induced by shRNA transduction

Genes/genotypes		V	P	5	5P	A	A5	AP	A5P
shRNA	shAPCs					+	+	+	+
	shp53			+	+		+		+
	shPTEN		+		+			+	+
	pLKO.1	+							
IEC	WT	0/14	0/4	0/5	0/3	7/11	8/8	10/10	1/1
	$p53^{-/-}$	0/4	0/2	—	—	2/2	—	4/4	—
	$PTEN^{-/-}$	0/1	—	—	—	—	1/1	—	—

—, not tested. V, P, 5, and A depict vector, shPTEN, shp53, and shAPCs, respectively.

MEDICAL SCIENCES

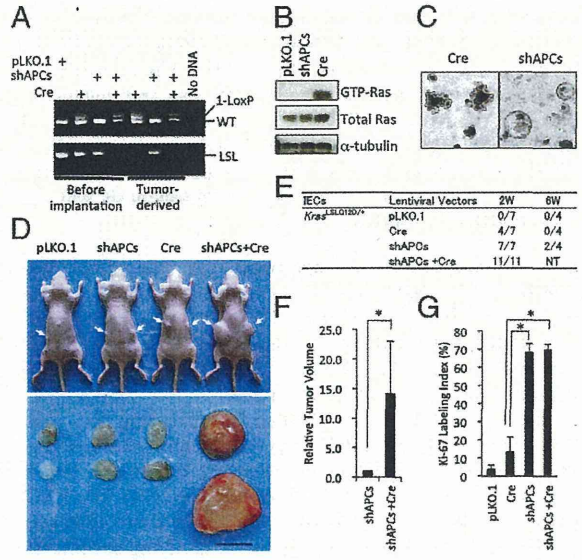

Fig. 4. Synergy between *APC* suppression and *Kras* activation in organoids for tumorigenesis. (*A*) Cre-mediated recombination in vitro. Genomic PCR analysis for WT and recombined allele of *Kras* (*Upper*) and for the LSL cassette (*Lower*). 1-LoxP, single LoxP after the recombination. (*B*) Enrichment of active Ras by induction of $Kras^{G12D}$. Immunoblotting analysis for Ras before (*Middle*) and after (*Top*) GST pulldown assay. α-Tubulin serves as a loading control (*Bottom*). (*C*) Transduced organoids in 3D culture. $Kras^{G12D}$ did not induce cystic shape. (*D*) s.c. tumors in nude mice. Palpable nodules (arrow) at 2 wk postinjection (*Upper*) and corresponding nodules after excision (*Lower*). (Scale bar, 10 mm.) (*E*) Summary of tumor development. Data at 2 and 6 wk after the implantation are shown. NT, not tested. (*F*) relative ratio of tumor volume. Mean ± SD (n = 7 each) is shown, $^*P < 0.01$. (*G*) Ki-67 labeling index for epithelia in the nodules. Mean ± SD is shown; $^*P < 0.01$. pLKO.1 (n = 3), Cre (n = 3), shAPCs (n = 7), and shAPCs+Cre (n = 7).

a few glands of ductal or cystic shape (Fig. 5 *A* and *D*), with impaired cell differentiation and proliferation as exemplified by loss of mucus production (Fig. 5*G*) and low Ki-67 index (Figs. 4*G* and 5*J*), respectively. Consistent with the lack of Wnt pathway activation (Fig. 4*C*), β-catenin remained in the membrane (Fig. 5*M*). $Kras^{G12D}$ nodule-derived organoids proved completely deleted for LSL, which had been only partially deleted when injected (Fig. 4*A*), suggesting their transient growth advantage. However, $Kras^{G12D}$ tumors no longer remained at 6 wk after injection (Fig. 4*E*), indicating that *Kras* activation by itself was insufficient for establishment of tumors, consistent with previous studies reporting no effect in the small intestine (13, 14, 36) and induction of only hyperplasia in the colon (15, 37). Also, initial proliferation and eventual extinction might mirror the natural course of aberrant crypt foci (ACF) (38), which are early lesions of the colon highly associated with *Kras* mutation (39).

Acquired Cancer Stem Cell–Like Properties in Tumor-Derived Organoids. As intestinal stem cells (ISCs) were unable to survive in s.c. tissue (Fig. 3*A*), development and maintenance of tumor glands with differentiated and proliferative properties (Fig. 3 *C* and *F*) suggested the emergence of a distinct subpopulation with the ability to self-renew and differentiate. To better characterize the nature of induced tumors, we harvested all of the nodules to conduct organoid cultures and obtained organonids only from tumors. *APC* and *PTEN* were suppressed by corresponding shRNAs (Fig. 6*A*), confirming successful transduction. Tumor-derived organoids proved tumorigenic in all seven cases examined. Notably, tumors from identical cells gave rise to secondary tumors akin to the primary tumors in both magnitude (Fig. 6*B*) and histology (Fig. S7*A*), regardless of genetic background (Fig. S7*B*), further implying the emergence of a cancer stem cell (CSC)-like subpopulation. Sphere-forming potential in suspension culture has been associated with stemness (40). Whereas single cells containing ISCs did not form spheres, tumor-derived organoids yielded spheroids (Fig. 6*C*) in all seven cases examined. Even never-implanted organoids with shAPCs alone formed spheroids (Fig. 6*C*), suggesting induction of the CSC-like properties even before injection into nude mice. Quantitative PCR (qPCR) analysis revealed up-regulation of CSC markers *CD44* and *CD133* (41) but not ISC markers *Lgr5* or *Bmi1* (42) in tumor-derived organoids (Fig. 6*D*). Despite up-regulation of *Axin2* and *CD44* in tumors, *c-Myc* or *CCND1* were not induced, suggesting selective activation of a subset of Wnt target genes toward acquisition of CSC properties. Taken together, these results supported the notion that ISC-containing organoids likely comprised a subpopulation with CSC-like properties through *APC* inactivation.

Discussion

To model human CRC, inactivation of *APC* and subsequent tumor development in the intestine have basically been achieved in mutant or gene-modified mice for *APC* (4). In contrast, we demonstrated that it could also be achieved without a genetically

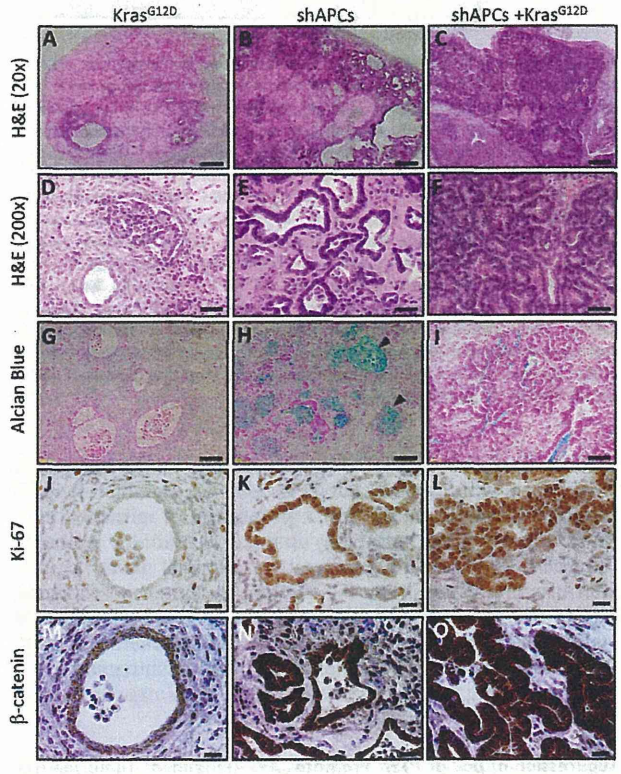

Fig. 5. Histological features of the tumors induced from $Kras^{LSL-G12D/+}$ organoids. (*A–F*) H&E staining at 20× (*A–C*) and 200× (*D–F*) magnification. (Scale bar, 500 and 50 μm, respectively.) (*G–I*) Alcian blue staining. No mucus production (*G*), formation of multiple mucus pool (closed arrowheads) in the stroma (*H*), and mucus confined in the lumen of intact glands (*I*). (Scale bar, 100 μm.) (*J–L*) Immunostaining for Ki-67. Few (*J*) and many (*K* and *L*) positive cells in the tumor glands are observed. (Scale bar, 25 μm.) (*M–O*) Immunostaining for β-catenin. Localized in the membrane (*M*), and accumulated in the cytoplasm or nucleus (*N* and *O*). (Scale bar, 25 μm.) Representative images are shown. Tumors were generated by $Kras^{G12D}$ (*Left*), shAPCs (*Center*), or both (*Right*) from identical cells and harvested at 2 wk after injection.

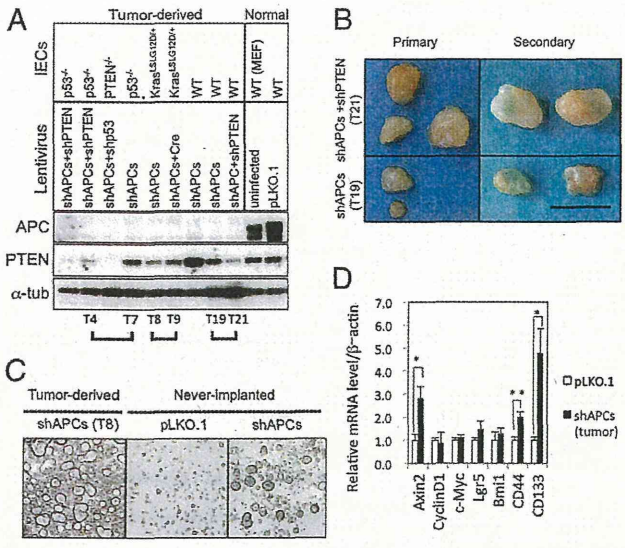

Fig. 6. Induction of cancer stem–like properties in tumors through *APC* suppression. (*A*) *APC* knockdown in tumors. Immunoblotting analysis of tumor-derived organoids for APC and PTEN. Mouse embryonic fibroblast (MEF) and normal IECs are positive controls. T4/7, T8/9, and T19/21 derived from identical primary cells, respectively. (*B*) Serial transplantation of tumors. s.c. tumors T19 (shAPCs) and T21 (shAPCs+shPTEN) in primary sites (*Left*) and corresponding secondary tumors after retransplantation (*Right*). (Scale bar, 10 mm.) (*C*) Sphere-forming assay. Representative images after 2-wk suspension culture are shown. (*D*) qPCR analysis for Wnt target genes and stem cell marker genes. Mean ± SD ($n = 3$) is shown; $^*P < 0.01$; $^{**}P < 0.05$.

engineered mouse, independently of intestinal microenvironment, and solely with primary IECs, providing an alternative way to model CRC in vitro. There were several issues to be resolved in the course of developing the model. First was to achieve stable transduction of stem cells, instead of gene targeting in embryonic stem (ES) cells. Despite initial technical difficulties, we eventually established a lentivirus-based transduction method, which was as simple as a routine subculture but highly efficient in obtaining stably transduced organoids. This methodological advantage was in sharp contrast to retroviral transduction of only cycling cells, with more complicated procedures but much less efficiency, definitely requiring drug selection to obtain stably transduced organoids (43). Both high infection efficiency and the growth advantage of inactivating tumor suppressors helped us conduct experiments without drug selection, which eliminated its potential side effects and enabled us to use vectors without selection markers or puro-resistant IECs from the *Kras*$^{LSLG12D/+}$ mouse (34). We further showed that Cre-mediated recombination of a floxed allele could be achieved in organoids. Thus, overexpression and knockdown could be simply achieved for many genes in WT IECs and gene disruption in conditionally gene-targeted IECs.

The second was in vitro expansion of *APC*-inactivated organoids. Inactivation of *APC* in the intestine is normally established by a stochastic second hit in heterozygous mice or by complete loss in mice homozygous for a floxed allele in a spatiotemporally regulated manner (22, 44, 45). Although rounded cystic organonids were available by 3D culture of *APC*-deficient adenoma developed in earlier studies (26, 27), *APC* loss and subsequent tumor development have been exclusively achieved in vivo, to which inflammation or interactions within the microenvironment might have played critical roles (17, 18). In some settings, tumor development itself could not be achieved due to organ failure induced immediately after *APC* loss (28). Thus, it was initially unclear whether we could achieve *APC* inactivation in organoids and its subsequent propagation thoroughly in vitro. IECs transduced with shAPC frequently failed to propagate, which might be partially in line with adverse effects caused by acute *APC* loss (28). We incidentally noted that this could be overcome by cointroducing all of the shAPC clones. A possible explanation could be that pooled shAPC clones yielded variations in the magnitude of Wnt activation, thereby increasing the probability of achieving the "just-right" signaling (46). Alternatively, cooperation among off-target effects by pooled clones could have contributed. Although the underlying mechanism remains to be investigated, organoids that grew out indeed carried shAPCs and phenocopied those derived from *APC*-deficient adenoma. Based on the high similarity, we reasoned that propagated organoids with shAPCs might likely be an in vitro equivalent to adenoma. We then took advantage of this situation for further analysis.

The third was the strict definition of tumor in this model, which was definitely required to relate the results to earlier studies in vivo. We tentatively defined tumors as nodules replacing coinjected Matrigel with proliferating epithelial glands at 6 wk postinjection. Only if tumors proved lethal at an earlier point were nodules exceptionally diagnosed on death. Accordingly, nonlethal nodules at 2 wk after injection were not treated as tumors. Acquisition of the potential for sphere formation and serial transplantation and induction of CSC markers were confirmed in tumor-derived organoids, clearly indicating that they had indeed undergone transformation. These results tend to support the validity of our definition of tumors.

With this experimental system, the relevance of known genetic alterations in CRC could be essentially recapitulated, either individually or in the context of *APC* loss, as in *PTEN* loss (11, 12) and *Kras* activation (13–15, 36, 37). With regard to *p53* loss, its genetic cooperation with *APC* loss was negative in the heterogeneous genetic background (31, 47) but proved to be positive in a congenic background (9, 10), consistent with this study. These findings highlight the relevance of conducting the analysis on genetic interaction in exactly the same genetic background as achieved in our model, which otherwise requires multiple backcrossing. Thus, validation of candidate genes or genetic cooperation will be warranted, leading to quick identification of the genes to be prioritized for further investigations from many candidates (19, 20) before, or even without, generation of gene-modified mice. Also, generation of tumors with defined genotypes could be facilitated. The custom-made "genetically clean" cell lines would become valuable resources for identification of effective compounds or therapeutic targets by high-throughput screening or in preclinical studies.

Considering similarities in outcome and approach, our in vitro model might well be comparable to those two types of in vivo studies, in which *APC* was subject to acute deletion in the intestine, rather than studies with the *APC*-heterozygous mutant mouse (15). One is *APC* loss in an Lgr5$^+$ stem cell–specific manner, which quickly gives rise to adenoma (22, 26, 48). The other is *APC* loss either focally or entirely in the intestine. Local injection of adenovirus-Cre induced adenoma in the distal colon, although transduction was achieved in only a limited area (44, 45). Cre-mediated inducible and acute loss of APC throughout the intestine led to morbidity within 5 d (28), but the crypts that were rescued by harvesting 2 d after APC loss proved tumorigenic in nude mice (49). In both cases, *APC* inactivation was achieved in gene-modified mice in vivo, presumably by cooperating with the microenvironment. Besides, special conditions such as cell type–specific gene ablation or crypt harvest at specific times were necessary. In contrast, in our model, *APC* inactivation was simply achieved in WT IECs in vitro, without any other type of cells or experimental conditions, obviously facilitating intestinal tumorigenesis studies. As organoid culture is optimized for Lgr5$^+$ stem cells (24), it is conceivable that Lgr5$^+$ stem cells were predominantly transformed in our model. On the other hand,

lentiviral transduction could also target quiescent stem cells, which could be marked by Bmi1 (42), Lrig1 (50), mTert (51), or HopX (52), in a mutually overlapping but distinct manner. Moreover, even Lgr5$^-$ differentiated cells could dedifferentiate to reacquire stem cell properties and initiate tumorigenesis (49). Thus, there is a possibility that tumor initiation could take place through many different pathways, including reprogramming of nonstem cells. In this regard, our model might provide unique opportunities in addressing this issue in an unbiased way, as the entire process of tumorigenesis could be simply recapitulated without predefined conditions on tumor-initiating cells.

In conclusion, we developed a unique in vitro model for CRC, with which genetic interactions in both tumor initiation and progression will be simply but genuinely analyzed. By serving as an alternative or complement to the standard approaches, it would likely accelerate CRC research.

Materials and Methods

Singly dissociated intestinal cells were lentivirally transduced in vitro. Organoids were maintained for 4 wk in Matrigel and injected into nude mice to evaluate tumorigenicity. Several weeks after the implantation, the tumors were subjected to histological analysis or 3D culture to obtain a pure population of tumor-derived organoids, which were further analyzed by Western blotting, qPCR, and sphere-forming assay. Extended materials and methods are available in *SI Materials and Methods*.

ACKNOWLEDGMENTS. We thank the Core Facility Division and Central Animal Division in the National Cancer Center Research Institute for technical support in histological and animal studies, respectively. We thank Elaine Fuchs for providing LV-Cre pLKO.1, Hiroshi Ohshima for *p53*-mutant mice, and Akira Suzuki for *PTEN* floxed mice. We also thank Ibuki Kobayashi and Sachiko Dobashi for technical assistance. This study was supported by Grants-in-Aid for the Third Term Comprehensive 10-Year Strategy for Cancer Control from the Ministry of Health, Labor and Welfare of Japan and a grant from the Japan Chemical Industry Association Long Range Research Initiative. K. Onuma was a recipient of the Research Resident Fellowship from the Foundation for Promotion of Cancer Research (Japan).

1. Markowitz SD, Bertagnolli MM (2009) Molecular origins of cancer: Molecular basis of colorectal cancer. *N Engl J Med* 361(25):2449–2460.
2. Walther A, et al. (2009) Genetic prognostic and predictive markers in colorectal cancer. *Nat Rev Cancer* 9(7):489–499.
3. Aoki K, Taketo MM (2007) Adenomatous polyposis coli (APC): A multi-functional tumor suppressor gene. *J Cell Sci* 120(Pt 19):3327–3335.
4. Taketo MM, Edelmann W (2009) Mouse models of colon cancer. *Gastroenterology* 136(3):780–798.
5. Tanaka T (2009) Colorectal carcinogenesis: Review of human and experimental animal studies. *J Carcinog* 8:5.
6. Takahashi M, Nakatsugi S, Sugimura T, Wakabayashi K (2000) Frequent mutations of the beta-catenin gene in mouse colon tumors induced by azoxymethane. *Carcinogenesis* 21(6):1117–1120.
7. Nakagama H, Nakanishi M, Ochiai M (2005) Modeling human colon cancer in rodents using a food-borne carcinogen, PhIP. *Cancer Sci* 96(10):627–636.
8. Tsuchiya N, et al. (2007) SND1, a component of RNA-induced silencing complex, is up-regulated in human colon cancers and implicated in early stage colon carcinogenesis. *Cancer Res* 67(19):9568–9576.
9. Halberg RB, et al. (2008) The pleiotropic phenotype of Apc mutations in the mouse: Allele specificity and effects of the genetic background. *Genetics* 180(1):601–609.
10. Halberg RB, et al. (2000) Tumorigenesis in the multiple intestinal neoplasia mouse: Redundancy of negative regulators and specificity of modifiers. *Proc Natl Acad Sci USA* 97(7):3461–3466.
11. Marsh V, et al. (2008) Epithelial Pten is dispensable for intestinal homeostasis but suppresses adenoma development and progression after Apc mutation. *Nat Genet* 40(12):1436–1444.
12. Shao J, Washington MK, Saxena R, Sheng H (2007) Heterozygous disruption of the PTEN promotes intestinal neoplasia in APCmin/+ mouse: Roles of osteopontin. *Carcinogenesis* 28(12):2476–2483.
13. Janssen KP, et al. (2006) APC and oncogenic KRAS are synergistic in enhancing Wnt signaling in intestinal tumor formation and progression. *Gastroenterology* 131(4): 1096–1109.
14. Sansom OJ, et al. (2006) Loss of Apc allows phenotypic manifestation of the transforming properties of an endogenous K-ras oncogene in vivo. *Proc Natl Acad Sci USA* 103(38):14122–14127.
15. Haigis KM, et al. (2008) Differential effects of oncogenic K-Ras and N-Ras on proliferation, differentiation and tumor progression in the colon. *Nat Genet* 40(5):600–608.
16. Tanaka T, et al. (2006) Dextran sodium sulfate strongly promotes colorectal carcinogenesis in Apc(Min/+) mice: Inflammatory stimuli by dextran sodium sulfate results in development of multiple colonic neoplasms. *Int J Cancer* 118(1):25–34.
17. Rakoff-Nahoum S, Medzhitov R (2007) Regulation of spontaneous intestinal tumorigenesis through the adaptor protein MyD88. *Science* 317(5834):124–127.
18. Musteanu M, et al. (2010) Stat3 is a negative regulator of intestinal tumor progression in Apc(Min) mice. *Gastroenterology* 138(3):1003–1011.
19. Cancer Genome Atlas Network (2012) Comprehensive molecular characterization of human colon and rectal cancer. *Nature* 487(7407):330–337.
20. Bass AJ, et al. (2011) Genomic sequencing of colorectal adenocarcinomas identifies a recurrent VTI1A-TCF7L2 fusion. *Nat Genet* 43(10):964–968.
21. Starr TK, et al. (2009) A transposon-based genetic screen in mice identifies genes altered in colorectal cancer. *Science* 323(5922):1747–1750.
22. Barker N, et al. (2009) Crypt stem cells as the cells-of-origin of intestinal cancer. *Nature* 457(7229):608–611.
23. Zhu L, et al. (2009) Prominin 1 marks intestinal stem cells that are susceptible to neoplastic transformation. *Nature* 457(7229):603–607.
24. Sato T, et al. (2009) Single Lgr5 stem cells build crypt-villus structures in vitro without a mesenchymal niche. *Nature* 459(7244):262–265.
25. Case SS, et al. (1999) Stable transduction of quiescent CD34(+)CD38(-) human hematopoietic cells by HIV-1-based lentiviral vectors. *Proc Natl Acad Sci USA* 96(6):2988–2993.
26. Sato T, et al. (2011) Long-term expansion of epithelial organoids from human colon, adenoma, adenocarcinoma, and Barrett's epithelium. *Gastroenterology* 141(5): 1762–1772.
27. Sato T, et al. (2011) Paneth cells constitute the niche for Lgr5 stem cells in intestinal crypts. *Nature* 469(7330):415–418.
28. Sansom OJ, et al. (2004) Loss of Apc in vivo immediately perturbs Wnt signaling, differentiation, and migration. *Genes Dev* 18(12):1385–1390.
29. Jho EH, et al. (2002) Wnt/beta-catenin/Tcf signaling induces the transcription of Axin2, a negative regulator of the signaling pathway. *Mol Cell Biol* 22(4):1172–1183.
30. Donehower LA, et al. (1992) Mice deficient for p53 are developmentally normal but susceptible to spontaneous tumours. *Nature* 356(6366):215–221.
31. Clarke AR, Cummings MC, Harrison DJ (1995) Interaction between murine germline mutations in p53 and APC predisposes to pancreatic neoplasia but not to increased intestinal malignancy. *Oncogene* 11(9):1913–1920.
32. Roberts RB, et al. (2002) Importance of epidermal growth factor receptor signaling in establishment of adenomas and maintenance of carcinomas during intestinal tumorigenesis. *Proc Natl Acad Sci USA* 99(3):1521–1526.
33. Beronja S, Livshits G, Williams S, Fuchs E (2010) Rapid functional dissection of genetic networks via tissue-specific transduction and RNAi in mouse embryos. *Nat Med* 16(7): 821–827.
34. Tuveson DA, et al. (2004) Endogenous oncogenic K-ras(G12D) stimulates proliferation and widespread neoplastic and developmental defects. *Cancer Cell* 5(4):375–387.
35. Jackson EL, et al. (2001) Analysis of lung tumor initiation and progression using conditional expression of oncogenic K-ras. *Genes Dev* 15(24):3243–3248.
36. Ray KC, et al. (2011) Epithelial tissues have varying degrees of susceptibility to Kras (G12D)-initiated tumorigenesis in a mouse model. *PLoS ONE* 6(2):e16786.
37. Feng Y, et al. (2011) Mutant KRAS promotes hyperplasia and alters differentiation in the colon epithelium but does not expand the presumptive stem cell pool. *Gastroenterology* 141(3):1003–1013.
38. Raju J (2008) Azoxymethane-induced rat aberrant crypt foci: Relevance in studying chemoprevention of colon cancer. *World J Gastroenterol* 14(43):6632–6635.
39. Yamashita N, Minamoto T, Ochiai A, Onda M, Esumi H (1995) Frequent and characteristic K-ras activation and absence of p53 protein accumulation in aberrant crypt foci of the colon. *Gastroenterology* 108(2):434–440.
40. Pastrana E, Silva-Vargas V, Doetsch F (2011) Eyes wide open: A critical review of sphere-formation as an assay for stem cells. *Cell Stem Cell* 8(5):486–498.
41. Wang C, et al. (2012) Evaluation of CD44 and CD133 as cancer stem cell markers for colorectal cancer. *Oncol Rep* 28(4):1301–1308.
42. Yan KS, et al. (2012) The intestinal stem cell markers Bmi1 and Lgr5 identify two functionally distinct populations. *Proc Natl Acad Sci USA* 109(2):466–471.
43. Koo BK, et al. (2012) Controlled gene expression in primary Lgr5 organoid cultures. *Nat Methods* 9(1):81–83.
44. Shibata H, et al. (1997) Rapid colorectal adenoma formation initiated by conditional targeting of the Apc gene. *Science* 278(5335):120–123.
45. Hung KE, et al. (2010) Development of a mouse model for sporadic and metastatic colon tumors and its use in assessing drug treatment. *Proc Natl Acad Sci USA* 107(4): 1565–1570.
46. Albuquerque C, et al. (2002) The 'just-right' signaling model: APC somatic mutations are selected based on a specific level of activation of the beta-catenin signaling cascade. *Hum Mol Genet* 11(13):1549–1560.
47. Fazeli A, et al. (1997) Effects of p53 mutations on apoptosis in mouse intestinal and human colonic adenomas. *Proc Natl Acad Sci USA* 94(19):10199–10204.
48. Schepers AG, et al. (2012) Lineage tracing reveals Lgr5+ stem cell activity in mouse intestinal adenomas. *Science* 337(6095):730–735.
49. Schwitalla S, et al. (2013) Intestinal tumorigenesis initiated by dedifferentiation and acquisition of stem-cell-like properties. *Cell* 152(1-2):25–38.
50. Powell AE, et al. (2012) The pan-ErbB negative regulator Lrig1 is an intestinal stem cell marker that functions as a tumor suppressor. *Cell* 149(1):146–158.
51. Montgomery RK, et al. (2011) Mouse telomerase reverse transcriptase (mTert) expression marks slowly cycling intestinal stem cells. *Proc Natl Acad Sci USA* 108(1): 179–184.
52. Takeda N, et al. (2011) Interconversion between intestinal stem cell populations in distinct niches. *Science* 334(6061):1420–1424.

Biochemical and Biophysical Research Communications 443 (2014) 852–857

Contents lists available at ScienceDirect

Biochemical and Biophysical Research Communications

journal homepage: www.elsevier.com/locate/ybbrc

AKT is critically involved in cooperation between obesity and the dietary carcinogen amino-1-methyl-6-phenylimidazo [4,5-*b*] (PhIP) toward colon carcinogenesis in rats

Maki Igarashi[1], Yoshitaka Hippo*, Masako Ochiai, Hirokazu Fukuda, Hitoshi Nakagama

Division of Cancer Development System, National Cancer Center Research Institute, 5-1-1 Tsukiji, Chuo-ku, Tokyo 104-0045, Japan

ARTICLE INFO

Article history:
Received 6 December 2013
Available online 14 December 2013

Keywords:
Colon cancer
Rat
Susceptibility
Obesity
PhIP
AKT

ABSTRACT

Obesity is highly associated with colon cancer development. Whereas it is generally attributed to pro-tumorigenic effects of high fat diet (HFD), we here show that a common genetic basis for predisposition to obesity and colon cancer might also underlie the close association. Comparison across multiple rat strains revealed that strains prone to colon tumorigenesis initiated by a dietary carcinogen amino-1-methyl-6-phenylimidazo [4,5-*b*] pyridine (PhIP) tended to develop obesity. Through transcriptome and extensive immunoblotting analyses, we identified the basal level of activated AKT in colonic crypts as a biomarker for the common predisposition. Notably, PhIP induced activation of AKT, which could persist for several weeks under a low fat diet (LFD), but not under HFD. On the other hand, PhIP and HFD independently induced Wnt pathway activation and inhibited apoptosis, through distinct mechanisms involving GSK-3β, caspase 3 and poly-ADP ribose polymerase (PARP). Taken together, these observations provide mechanistic insights into how PhIP-induced activation of AKT might cooperate with HFD at multiple levels toward development of colon cancer.

1. Introduction

Colorectal cancer (CRC) is a leading cause of cancer death worldwide [1]. In the multi-step development of sporadic CRC, Wnt pathway activation is the most frequent initiating event, typically achieved by functional loss of adenomatous polyposis coli (APC) or activating mutation of CTNNB1 encoding β-catenin [2]. Subsequent progression to full-blown tumors is mediated by accumulation of genetic alterations in tumor suppressor genes and oncogenes [3], or by environmental factors, including inflammation. In fact, inflammatory bowel disease is a high-risk condition for CRC in humans [4], and dextran sodium sulfate (DSS)-induced colitis accelerates azoxymethane-induced colon tumorigenesis in mice [5]. Obesity-associated visceral fat or adipocytes have recently emerged as a source of inflammation [6]. Leptin and adiponectin, a class of cytokines secreted by adipocytes, are mediators of inflammation by binding to their specific receptors [7]. Genetic ablation of these pathways in mice indeed affected tumorigenicity under a high fat diet (HFD), confirming the pro-tumorigenic nature of obesity [8,9].

Amino-1-methyl-6-phenylimidazo [4,5-*b*] pyridine (PhIP) is a heterocyclic amine (HCA) abundantly contained in cooked meat. It binds to DNA and forms adducts, which could in turn induce mutations, thereby potently inducing tumors in the colon, prostate and mammary glands in rats [10]. Notably, these types of tumors are all closely associated with westernized high-fat diets in humans, and HFD indeed accelerated PhIP-initiated carcinogenesis in these organs in rats [11]. PhIP administration recapitulates multi-step colon tumorigenesis from aberrant crypt foci (ACF), dysplasia, adenoma, and adenocarcinoma [12]. Besides, PhIP-induced tumors frequently harbor mutations in APC and CTNNB1, similar to human CRC [13]. These observations strongly suggested that PhIP might be a major environmental carcinogen for human CRC.

Although ACF are not *bona fide* pre-neoplastic lesions of the colon, susceptibility of strains to chemically-induced tumorigenesis is conveniently estimated by the number of ACF at an early point, largely due to their high correlation, shorter period of time for observation, and higher incidence [14]. The numbers of ACF induced by PhIP vary among inbred strains [12], strongly suggesting that multiple genetic factors determine the susceptibility to colon carcinogenesis. In an effort to identify these loci, we noted that rat strains with more ACF tended to manifest a more severe obese phenotype, which prompted us to investigate the molecular

Abbreviations: PhIP, amino-1-methyl-6-phenylimidazo [4,5-*b*] pyridine; HCA, heterocyclic amine; ACF, aberrant crypt foci; GSEA, gene set enrichment analysis.

* Corresponding author. Fax: +81 3 3542 2530.
E-mail address: yhippo@ncc.go.jp (Y. Hippo).
[1] Present address: Department of Molecular Endocrinology, National Research Institute for Child Health and Development, 2-10-1 Okura, Setagaya-ku, Tokyo 157-8535, Japan.

0006-291X/$ - see front matter © 2013 Elsevier Inc. All rights reserved.
http://dx.doi.org/10.1016/j.bbrc.2013.12.059

basis underlying the common predisposition. We clarified the relevance of AKT in the colonic crypts in linking obesity to PhIP-induced CRC, providing mechanistic insights into the cooperation between obesity and CRC.

2. Materials and methods

2.1. Rats, diet and chemicals

We purchased BUF, F344 and ACI rats from CLEA Japan (Tokyo, Japan), LEW, WKY and BN from Charles River Japan Inc. (Yokohama, Japan), and WKAH, OM, DA and KND from Japan SLC (Hamamatsu, Japan). PVG, DON, LEA, DRH, WF, SDJ, LE and NIG-III were provided from The National BioResource Project (NBRP) for the Rat (Kyoto University, Kyoto, Japan). Animal studies were carried out according to the Guideline for Animal Experiments, drawn up by the Committee for Ethics in Animal Experimentation of the National Cancer Center, which meet the ethical standards required by the law and the guidelines about experimental animals in Japan. Five-week-old male rats were fed a low fat diet (LFD) AIN-93G (Dyets Inc., Bethlehem, PA) for 1 week. To induce ACF, rats were fed LFD containing 400 ppm of amino-1-methyl-6-phenylimidazo [4,5-*b*] pyridine (PhIP) (Nard Institute, Osaka, Japan) for the first 2 weeks, followed by a high fat diet (HFD) containing hydrogenated oil PRIMEX (Dyets) for 4 weeks. To induce tumors, this cycle was repeated three times, and experimental animals were fed a HFD for the rest of the course of experiments, to conduct an intermittent PhIP feeding protocol [11]. N-acetoxy-PhIP (Nard Institute), an active form of PhIP, was used for an *in vitro* experiment.

2.2. Evaluation of obesity and tumorigenicity

After fasting for 16 h, serum and body fat were collected on sacrifice at 12 weeks of age. All the blood biochemistry data were obtained by SRL Inc. (Tokyo, Japan). Body weight and body fat weight were measured at 8, 10, and 12 weeks of age. Visceral fat was harvested from epididymal, mesenteric, perirenal and retroperitoneal fat pads. Subcutaneous fat was collected from the dorsal skin. Total body fat weight was calculated as the sum of visceral and subcutaneous fats. The colons were fixed by 10% neutralized formalin overnight and stained with 0.2% methylene blue for 15 min to count the numbers of ACF, aberrant crypts (ACs), and tumors under a stereoscope. Paraffin-embedded thin sections at 5 μm were subject to hematoxylin and eosin staining for histological analysis.

2.3. Colon crypt isolation

Colonic fragments of 1–2 cm long were washed several times with TBS, and subject to incubation at 37 °C for 30 min in Hanks' balanced salt solution supplemented with 30 mM EDTA, 5 mM PMSF, 40 mM NaF and 5 mM sodium pyrophosphate decahydrate. Isolated crypts were stored at −80 °C until used for further analysis. RNA was extracted with TRIzol reagent (Invitrogen, Tokyo, Japan). Protein was extracted with T-PER Tissue Protein Extraction Reagent (Pierce, Alabama) supplemented with Complete Mini (Roche Diagnostics, Mannheim, Germany) and Halt Phosphatase Inhibitor (Pierce).

2.4. Cell culture

Normal human colon cells FHC were cultured in media containing 10% FBS and supplemented with penicillin and streptomycin. 1 day prior to experiments, the culture supernatant was replaced with serum-free media. N-acetoxy-PhIP, an activated form of PhIP, was dissolved in DMSO and added to the cells at 10 μM.

2.5. Microarray analysis

Labeled cDNA synthesized from 500 ng of total RNA was hybridized with Agilent Whole Rat Genome 4x44K microarrays, G4131F (Agilent Technologies), following the manufacturer's instructions. Hybridization images were scanned by High Resolution Microarray Scanner (Agilent Technologies), and analyzed with Agilent Feature Extraction Software v9.5. Raw data were analyzed by Gene Spring GX 7.3.1. Gene set enrichment analysis (GSEA) was conducted with GSEA software [15].

2.6. Western blotting

The proteins were separated by SDS–PAGE and transferred to PVDF membranes. The primary antibodies against p-AKT (Ser473), AKT, FOXO1, FOXO3a, FOXO4, Bim, Caspase-3, p-GSK3β (Ser9), GSK3β, p-β-catenin (Ser33/37/The41) and non-p-β-catenin (Ser33/37/Thr41) were purchased from Cell Signaling Technology (Danvers, MA), and those against β-catenin and c-myc were purchased from BD Transduction Laboratories (Lexington, KY) and Santa Cruz Biotechnology Inc., (Santa Cruz, CA), respectively. After incubation with HRP-conjugated secondary antibodies, images were visualized by enhanced chemiluminescence (Pierce). Signal intensity for p-AKT and total AKT was quantified by LAS3000 (Fujifilm, Tokyo, Japan).

2.7. Statistical analysis

All data are shown as mean ± SD. Statistical significance was determined by Mann–Whitney's *U*-test with the software JMP 9.0 (SAS Institute Japan, Tokyo, Japan). *p*-values less than 0.05 were considered significant.

3. Results

3.1. F344 rats are more susceptible to PhIP-induced colon tumorigenesis and obesity than ACI rats

Whereas carcinogenicity of chemicals is generally correlated with the number of ACF induced at an early point [16], this relationship remains elusive for PhIP. To address this issue, we chronologically monitored the colons from two rat strains treated with an intermittent PhIP-feeding protocol [11] (Fig. 1A). The numbers of both ACF and aberrant crypts (ACs) were significantly higher in the F344 rats compared to those in ACI rats at 12 weeks of age (Fig. 1B), consistent with a previous report [12]. At later time points, the number of ACs was still significantly higher in the F344 rats than in the ACI rats, but not with ACF. At 38 weeks of age, the number of colon tumors was significantly higher in F344 rats (Fig. 1C). In addition, the total number of dysplastic ACF, adenoma and adenocarcinoma were all higher in F344 rats. These results clearly indicated that the F344 rats more potently develop more advanced lesions than the ACI rats at any time point. Consequently, we reasoned that the number of ACF at 12 weeks of age would in fact serve as a marker to estimate tumor susceptibility of the strain and was used in subsequent analyses.

While examining ACF, we noted that the F344 rats tended to have more fat than the ACI rats. To verify this notion, we strictly quantified the fat weight of both strains at 6–12 weeks of age under LFD. Despite the similar level of body weight, a significantly higher degree of fat deposition was observed in F344 rats (Fig. 1D). This was also the case for visceral and subcutaneous fat. Severe accumulation of visceral fat has been associated with metabolic syndrome, which is characterized by hyperlipidemia, hypercholesterolemia and type II diabetes [17]. We then conducted

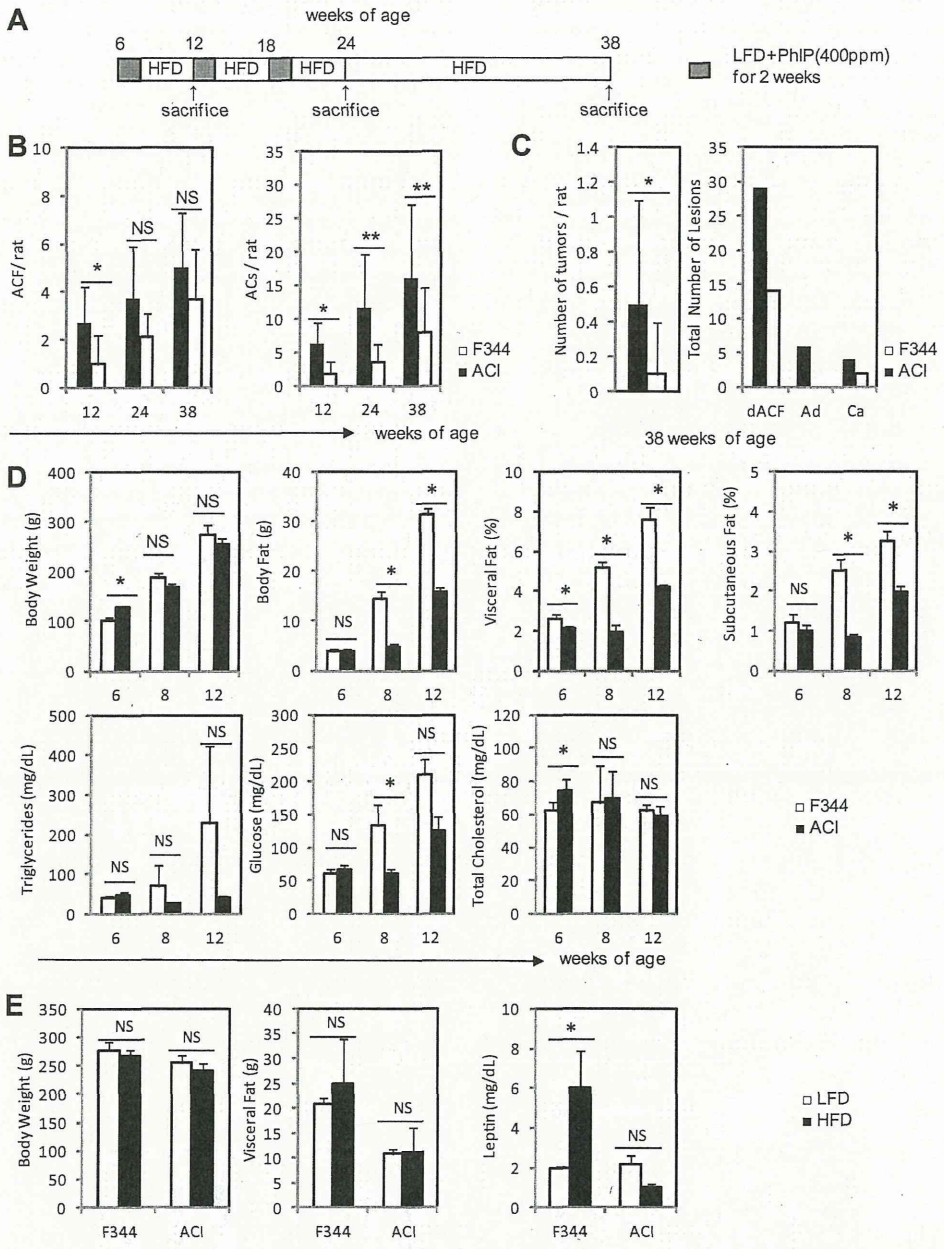

Fig. 1. Higher susceptibility to PhIP-induced colon tumorigenesis and obesity in F344 rats than in ACI rats. (A) A schematic view of the intermittent protocol for PhIP-induced colon carcinogenesis. (B) Time-series analysis of the number of ACF and ACs. The colons were examined at 12 (n = 10 each), 24 (n = 10 each), and 38 (n = 20 each) weeks of age. (C) Total number of tumors at 38 weeks of age. Both adenoma and carcinoma were counted as tumors. dACF, dysplastic ACF. Ad, adenoma. Ca, adenocarcinoma. (D) Time series analysis of body fat weight and blood biochemistry. Rats under LFD were sacrificed at 6 (n = 4 each), 8 (n = 4 each), and 12 (n = 3 each) weeks of age. (E) The effects of HFD on obesity. F344 (n = 4 each) and ACI (n = 5 each) rats under LFD or HFD for 6 weeks were sacrificed at 12 weeks of age. *p < 0.05 NS, not significant.

a blood biochemistry test and found that the level of serum triglycerides (TG) and glucose, but not total cholesterol, tended to be higher in F344 (Fig. 1D). Given that PhIP-induced colon carcinogenesis is promoted by HFD, we examined the effects of 6-week HFD on obesity. During 6–12 weeks of age, neither body weight nor the amount of visceral fat was affected in either strain (Fig. 1E). By contrast, the level of serum leptin significantly increased in F344 rats under HFD (Fig. 1E), in line with increased fat intake and ruling out the possibility that rats were improperly fed. These results indicated that F344 rats are inherently more prone to both CRC and obesity than ACI rats, which could be evaluated by measuring ACF and TG at 12 weeks of age.

3.2. Correlation between the magnitude of obesity and the incidence of ACF across multiple strains

We wondered if the observed correlation between predisposition to obesity and CRC could be more generalized. In an effort to identify genetic determinants of susceptibility to PhIP-induced CRC, we had characterized a total of 18 independent rat strains in terms of incidence of ACF under HFD for 4 weeks and collected blood samples, albeit under non-fasting conditions, from rats under LFD for 4 weeks (Fig. 2A). Although these data and samples may not be ideal for accurate analysis, we took advantage of this situation to gain insights into the common predisposition. Plotting the incidence of ACF (Fig. 2B)